THE ASTROPHYSICAL JOURNAL, 494:828–839, 1998 February 20

ON CHROMOSPHERIC HEATING MECHANISMS OF "BASAL FLUX" STARS[1]

P. G. JUDGE
High Altitude Observatory, National Center for Atmospheric Research,[2] P.O. Box 3000, Boulder CO 80307-3000
AND
K. G. CARPENTER
Laboratory for Astronomy and Solar Physics, Code 681, NASA Goddard Space Flight Center, Greenbelt, MD 20771
Received 1997 June 3; accepted 1997 September 30

ABSTRACT

Several pieces of evidence have been pieced together over recent years to support the notion that the chromospheric emission measured from stars with convection zones results in part from the upward propagation and dissipation of acoustic waves. One argument, based on a statistical analysis of available UV data of such stars across the H-R diagram, suggests the presence of an omnipresent "basal" level of chromospheric heating, which has been postulated as resulting from nonlinear acoustic wave heating.

However, with few exceptions, no studies have been made that test more directly the intrinsically dynamic nature of this shock-heating mechanism. Therefore, in order to search for more direct signatures of such upward-propagating shock waves in lines of C II, we examined Goddard High-Resolution Spectrograph spectra of several evolved stars that have "basal" levels of activity. No evidence is found to support the presence of such waves as a dominant component of the heating mechanism. Instead, behavior reminiscent of the solar transition region is seen, suggesting a magnetic heating mechanism for these stars.

We conclude that upward-propagating shock waves do not dominate the observed radiative losses from chromospheres of stars exhibiting typical "basal" behavior, and we suggest that the nonmagnetic origin of the basal components of all convective stars must be called into question. New solar data from the SUMER instrument on *SOHO* also suggest problems with the acoustic-wave interpretation, although further work is warranted.

In the course of this work, we also found a simple explanation for previously noted discrepancies between calculated and observed ratios of C II lines in the spectrum of α Ori.

Subject headings: shock waves — stars: chromospheres — stars: interiors — Sun: chromosphere

1. INTRODUCTION

Recent years have seen a convergence of ideas with regard to at least one component of chromospheric heating for stars that possess convective envelopes (see the review by Schrijver 1995). This has arisen from a synthesis of spatially and temporally resolved solar spectral and magnetic field data with unresolved UV stellar spectra, which became widely available after the launch of the *International Ultraviolet Explorer* (*IUE*) satellite in 1978. For a wide variety of stars, with the Sun as a special and notable case, these data have suggested that a significant fraction of chromospheric heating occurs through the propagation of acoustic waves, naturally generated in the convection zone, into higher atmospheric layers, where they steepen into shocks and dissipate.

Statistical evidence for this "basal" component of chromospheric heating was found by Schrijver (1987). Following early work by Ayres, Marstad, & Linsky (1981) and Oranje (1986), Schrijver (1987) studied in more detail the relationships between the radiative flux densities of pairs of emission features formed in stellar chromospheres, transition regions, and coronae. Schrijver used statistical tests to investigate the hypothesis that the radiation losses in the sample of stars contained signatures of *two* components of heating in the outer atmospheres: a basal component that depends on only fundamental stellar parameters (effective temperature and gravity) and another, magnetically related, component that depends on rotation rates and convection zone properties. He noted that the "flux-flux" correlations improved substantially when a basal component was included in the analysis and that the magnitude of the basal component derived from such an analysis was in agreement with the observed minimum in radiative flux densities seen in slowly rotating stars. This work was subsequently expanded and confirmed in a larger study by Rutten et al. (1991). These points led Schrijver to suggest that the basal component be identified with a nonmagnetic, i.e., acoustic, heating mechanism. This hypothesis has been studied further to include solar work, and the current status is nicely summarized in a review article (Schrijver 1995).

The purpose of this paper is to analyze chromospheric data for a variety of stars whose emission is ostensibly dominated by the basal component. We will demonstrate that data for stars with basal levels of chromospheric heating are incompatible with line profiles expected from the presence of upward-propagating shock waves, following some preliminary (one-dimensional) calculations by Judge & Cuntz (1993). We argue that the acoustic heating mechanism is not a viable one for our target stars and that weak magnetic fields are, in fact,

[1] Based on observations with the NASA/ESA *Hubble Space Telescope*, which is operated by the Association of Universities for Research in Astronomy, Inc., under NASA contract NAS 5-26555.

[2] The National Center for Atmospheric Research is sponsored by the National Science Foundation.

likely to be more important in heating the chromospheres.

2. OBSERVATIONAL DATA

2.1. *Finding a More Direct Diagnostic of Acoustic Heating Mechanisms*

To test the acoustic heating hypothesis, we look for direct evidence of the upward-propagating shock waves in the spectra of suitable stars. In the following, we implicitly assume, as all previous calculations have done, that the shock waves propagate mainly radially outward from the star, and we will return to this assumption in § 3. Our choice of target stars and spectral regions is driven by the following considerations:

First, we note that the proposed mechanism is essentially *dynamic*. Thus, any comparison between observation and theory ought to be based on direct signatures of such dynamics and not on secondary attributes, such as spectral features that contain only indirect information on velocity fields. Since the stellar convection zones (unlike low-order radial pulsations, for example) cannot provide physically coherent drivers over stellar hemispheres, direct observation of the variability of spatially integrated line intensities that respond to the propagation of shock fronts is not a reasonable option (see, e.g., Judge & Cuntz 1993). Instead, we rely on spatially and temporally averaged line profiles.

Second, we note that we should choose strong optically thin lines, since otherwise blends and radiation transport effects (including the effects of winds that are even less well understood than chromospheric heating mechanisms; see, e.g., Holzer & MacGregor 1985) radically influence the interpretation of line profiles.

Third, we should employ lines that can contain information on the *direction* of the propagation of compressive waves. Judge (1994) and Wikstøl, Judge, & Hansteen (1997) showed that the profiles of density-sensitive emission-line pairs may, under suitable conditions, contain information on the direction of propagation of compressive waves in the brightest (and therefore most heated) structures on the star.

Fourth, we should choose targets whose heating is dominated by the basal component in the context of the statistical samples studied by Schrijver (1987) and Rutten et al. (1991) and whose rotation rates are slow enough to see the signatures of the shock waves. A slowly rotating F star on the main sequence may be a suitable target, but the observational signature is potentially masked by the unknown effect of a dynamo operating in a shallow convection zone (§ 2.5 of Schrijver 1995). Candidates among the M dwarfs are intrinsically too dim to study at high resolution, and no statistical sample exists with which to set a basal level of activity. This leads us to focus upon slowly rotating giant stars.

Last, we must (obviously) select stars for which such observations have been obtained at spectral resolutions sufficient to see the effects of wave propagation on line profiles. Given that calculated shock speeds do not exceed sound speeds, c_S, which are themselves less than 10 km s^{-1}, by a factor of 2 (see, e.g., Ulmschneider 1991), this limits us to data acquired by the Goddard High Resolution Spectrograph (GHRS) on the *Hubble Space Telescope* (*HST*).

Guided by these five criteria, we are led to analyze the five lines of the C II $2s2p^2\,{}^4P \rightarrow 2s^22p\,{}^2P^o$ intercombination multiplet near 2325 Å, which is seen strongly in emission in giant and supergiant stars. Table 1 lists ratios of the five lines in the multiplet discussed here, showing which ratios are sensitive to density. Table 2 lists the targets we have studied. Note that two targets have been observed more than once. All the K- and M-type stars listed have (or even define) basal levels of chromospheric emission (Judge & Stencel 1991). These stars are all likely to be slow rotators [$v \sin(i) \leq 3$ km s^{-1}], according to measured upper limits for rotational broadening in K giants (Smith & Dominy 1979) coupled with results of calculations of angular momenta in evolutionary models (Rutten & Pylyser 1988).

2.2. *Overview of Data and Data Reduction*

The data were acquired in a nominal fashion with no observing problems for all the stars, with the exception of the 1994 α Tau data that were taken under "Coarse Track" guiding, rather than "Fine Track" lock, and the 1996 α Tau data that accumulated about 25% less exposure time than requested because of a delay in acquiring "lock" on the guide stars. In both cases, the data look excellent. We thus infer that the telescope pointing was quite stable during the "Coarse Track" guiding in 1994. The 1996 observations have sufficient signal-to-noise ratio for the purposes of this paper, despite being shorter than planned for other purposes.

With the exception of the RR Tel data, where photometric accuracy was paramount, all data were taken through the Small Science Aperture (SSA) to optimize the fidelity of the line profiles and the precision of the measured radial velocities. Dedicated wavelength calibration exposures with the on-board platinum lamps (referred to as "wavecals") were also obtained close in time to each of the stellar observations. These allow us to determine the dispersion coefficients and absolute wavelengths of each of the stellar observations to an accuracy of better than 0.3 diode widths, corresponding to Doppler shift uncertainties of about 3 km s^{-1} in the medium-resolution ($R = \lambda/\Delta\lambda =$ 22,500) and about 1.5 km s^{-1} in the echelle ($R = \lambda/\Delta\lambda =$ 78,000) observations. To reduce the effects of thermal drift and geomagnetic interactions within the spectrograph further (see Soderblom 1993), the exposures were generally

TABLE 1

RATIOS OF LINES IN THE $2s2p^2\,{}^4P \rightarrow 2s^22p\,{}^2P^o$ MULTIPLET OF C II

	TRANSITION			
NAME	$J_u \rightarrow J_l$	$J_u \rightarrow J_l$	WAVELENGTHS (Å)	DIAGNOSTIC
R_1.....	$(\frac{5}{2}-\frac{3}{2})$	$(\frac{1}{2}-\frac{3}{2})$	2325.398/2328.122	N_e
R_2.....	$(\frac{5}{2}-\frac{3}{2})$	$(\frac{3}{2}-\frac{3}{2})$	2325.398/2326.930	N_e
R_3.....	$(\frac{1}{2}-\frac{1}{2})$	$(\frac{3}{2}-\frac{3}{2})$	2324.689/2326.930	N_e
R_4.....	$(\frac{3}{2}-\frac{3}{2})$	$(\frac{3}{2}-\frac{1}{2})$	2326.930/2323.500	A-values, optical depth
R_5.....	$(\frac{1}{2}-\frac{3}{2})$	$(\frac{1}{2}-\frac{1}{2})$	2328.122/2324.689	A-values, optical depth

TABLE 2

LOG OF GHRS OBSERVATIONS

Item	Target	Spectral Type	Date of Observation[a] (UT)	Exposure Time (minutes)	Mode[b]	Program
1.....	γ Dra	K5 III	1995 Jul 19 23:08	21.8	SSA/G270M	6068
2.....	α Tau	K5 III	1990 Nov 27 20:32	19.7	SSA/G270M	3032
3.....	α Tau	K5 III	1990 Nov 27 17:35	54.3	SSA/ECH-B	3032
4.....	α Tau	K5 III	1994 Apr 8 12:37	19.7	SSA/G270M	5358
5.....	α Tau	K5 III	1994 Apr 8 01:21	19.7	SSA/G270M	5358
6.....	α Tau	K5 III	1996 Oct 15 20:09	13.5	SSA/G270M	6722
7.....	γ Cru	M3 III	1992 Mar 24 20:21	14.8	SSA/G270M	3212
8.....	μ Gem	M3 IIIvar	1993 Sep 27 23:11	29.6	SSA/G270M	4685
9.....	g Her	M6 III	1995 May 6 21:51	43.1	SSA/G270M	4685
10.....	λ Vel	K5 Ib	1994 Sep 3 23:03	42.6	SSA/G270M	5359
11.....	α Ori	M2 Iab	1992 Sep 22 07:49	59.2	SSA/ECH-B	1199
12.....	α Ori	M2 Iab	1992 Sep 24 06:24	9.8	SSA/G270M	1199
13.....	TX Psc	C6.2	1994 Dec 4 07:36	178	SSA/G270M	5694
14.....	RR Tel[c]	Slow nova	1995 Jul 16 16:26	10.0	LSA/G270M	5863

[a] Start time.

[b] Aperture/grating combination used; for example, SSA/ECH-B implies small science aperture used with the echelle-B grating.

[c] This target was chosen as a control experiment; see text.

divided into a series of subexposures, each with an integration time of 5 minutes or less. These exposures allowed any drifts within the spectrograph to be measured and corrected for in the spectral reduction process.

The GHRS observations were calibrated with the CALHRS routine developed by the GHRS Investigation Definition Team. This program merges the individual samples into a single spectrum, subtracts background counts, and corrects for nonlinearities in detector sensitivity. It then corrects for vignetting and the echelle blaze function (if required) and applies an absolute flux calibration. The wavelength calibration was performed using the wavecal exposures associated with each science observation. Separate exposures (i.e., the "subexposures" referenced above) at a given wavelength were then cross-correlated and co-added to produce the final spectra. We estimate the final absolute flux calibration of the GHRS SSA spectra to be accurate to $\pm 5\%$–10% and that of the LSA spectra to $\pm 5\%$.

Figure 1 shows a collage of much of the analyzed data, using the medium-dispersion data (just one spectrum is plotted for the two stars with more than one spectrum acquired). Figure 2 shows spectra, normalized so that the maximum flux in the frame is equal to 1.0, taken at different epochs or with different modes for the same targets. Wavelengths in air are used throughout this paper. Several important features should be noted. For those targets with exposures using both the echelle and the medium-resolution gratings, it is clear that little extra information is contained in the echelle data. The lines are *much* broader than the theoretical resolution of the GHRS in medium dispersion. We therefore infer that GHRS medium-dispersion data have sufficient resolution to resolve the intrinsic stellar profiles for all giant and supergiant stars. Next, we notice that the data discussed by Judge (1994) appear to be typical of the star he considered (α Tau) and of our other stars (this will become even more apparent when the data are further scrutinized, below). Finally, we notice that data for the carbon star TX Psc not only are noisier than the rest but also reveal evidence for contamination (there is an obvious absorption feature in the C II 2325.4 Å line).

The data were subsequently processed in the same manner as discussed by Judge (1994). First, the wavelength scales were shifted to those in the photospheric rest frames. Photospheric radial velocities were taken from the SIMBAD database, which, with few exceptions, takes them from Wilson (1963). The uncertainties in photospheric velocities are at most 1 km s^{-1} for the nonvariable target stars but can be several km s^{-1} for the photometric variables. For example, the standard deviations of all data in the SIMBAD database for μ Gem and g Her are just 0.5 and 0.4 km s^{-1}, respectively, but are 4.4 and 1.5 km s^{-1} for TX Psc and α Ori, respectively. Between 1953 and 1972, the photospheric velocity of the variable star TX Psc changed from -11 to $+18$ km s^{-1}!

Next, we attempted to remove known blended lines using profiles of other lines in the spectra as templates, following Judge (1994). Two of the C II lines used in the density-sensitive diagnostic analysis are affected by the (opacity-broadened) wings of the strong Fe II line at 2327.397 Å. Weaker blended lines of Si II] λ2328.510 and Co II λ2324.317 were subtracted from the spectra using the template lines Si II λ2350.170 (where available) and Co II λ2330.358, respectively.

2.3. *Properties of Line Profiles*

All the observed lines are substantially broader than the point-spread functions of the GHRS. The full width at half-maximum (FWHM) of these lines is typically 20–25 km s^{-1}, compared with 13 km s^{-1} and 3.85 km s^{-1} for the grating and echelle modes, respectively (Heap et al. 1995). Assuming the lines are formed in regions where the electron temperature is less than 10^4 K (for justification, see, e.g., Judge 1986 for the case of α Tau), the line widths (now expressed as a most probable speed in a Gaussian distribution = FWHM/1.66) are 12–15 km s^{-1} and are thus also in excess of the thermal widths of ≤ 6.2 km s^{-1} and of the sound speed, which is less than 10 km s^{-1}.

Radial velocities of the frequency-integrated C II emission lines relative to the photospheric rest frames were derived in two ways. First we computed cross-correlation coefficients between a theoretical spectrum (simply a Gaussian-broadened spectrum at zero Doppler shift with relative intensities similar to those observed) with the spectra.

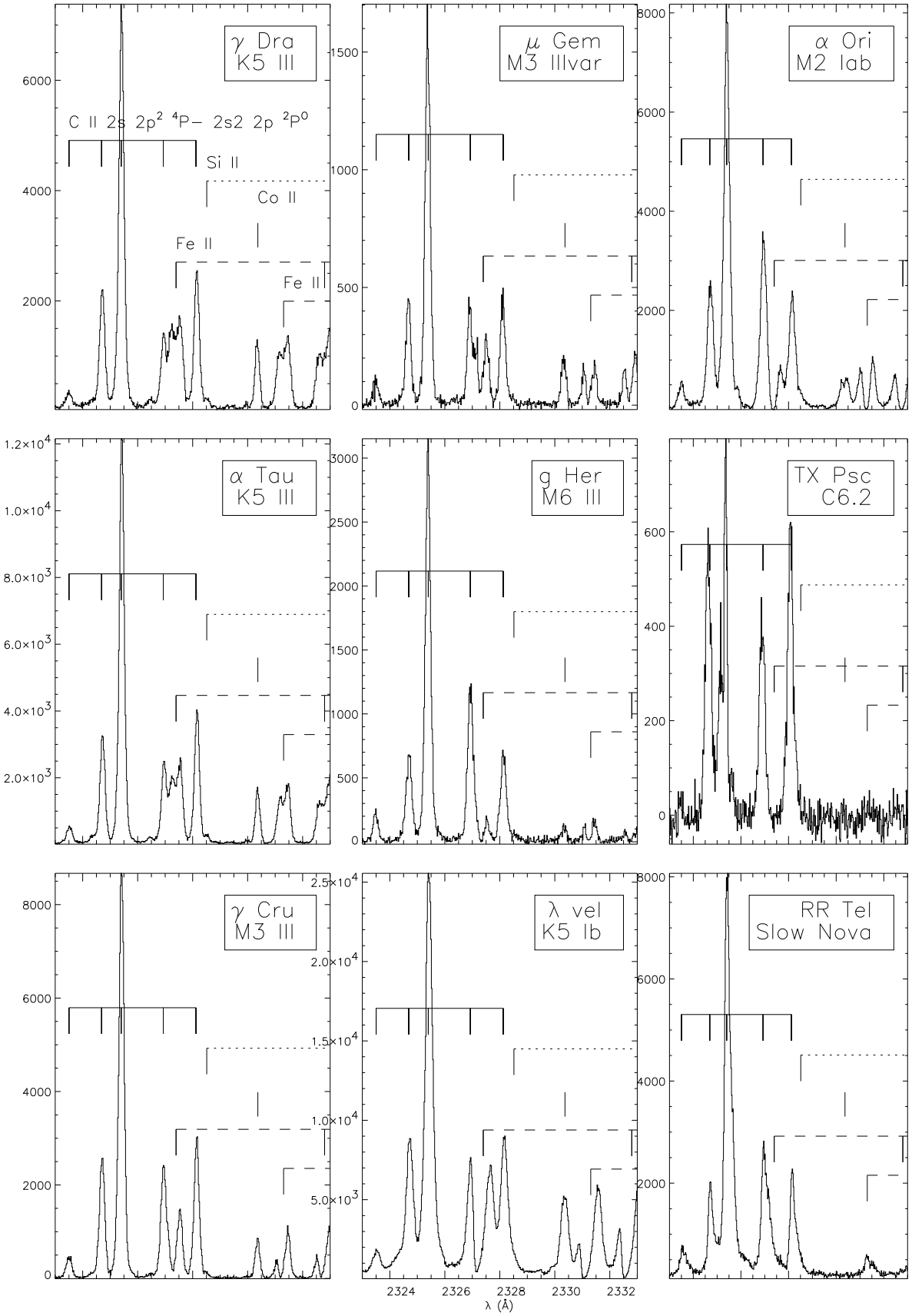

FIG. 1.—Spectra of the various target stars are shown with the region near 2330 Å containing the density-sensitive C II multiplet, highlighted. The ordinates give counts on the GHRS detector. All wavelengths are relative to the stellar photospheric rest frames.

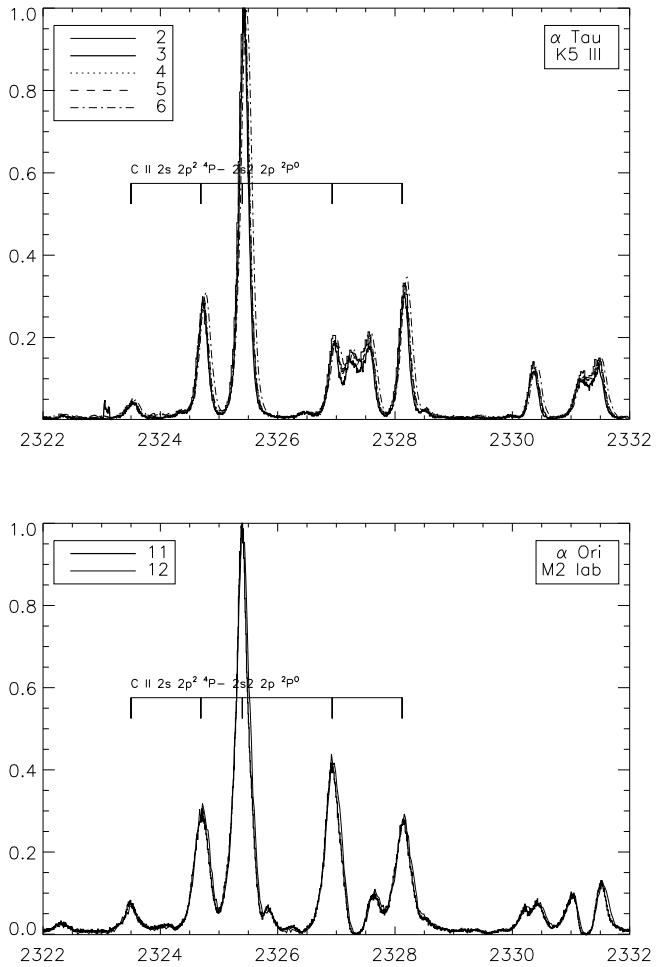

FIG. 2.—All spectra of the two target stars having multiple observations (α Tau and α Ori) are shown, normalized such that the peak is set to unity. The number in the legend refers to the item (row number) in Table 2. These data show small detailed changes as functions of time and as functions of the observing mode used (echelle mode versus the medium-dispersion mode).

Second, we fitted Gaussian line profiles to the lines. The results of the first method are listed in Table 3. The second method was used to assess likely uncertainties in the derived velocities from the spread of values derived for the five lines (including subtraction of the blended lines). This yielded a typical uncertainty of 0.5 km s^{-1} for all spectra, a negligible source of uncertainty compared with the ± 3 km s^{-1} GHRS wavelength calibration error. Taken together, the data in Table 3 are consistent with the picture that the frequency-integrated chromospheric C II emission is, for all stars with accurately determined photospheric radial velocities, always significantly redshifted. For the single star observed repeatedly (α Tau), we always find redshifts. One episode (in cycle 6) showed a significantly increased redshift.

Now we look in more detail at the line profiles. Figure 3 shows ratios of line profiles and inferred electron densities, computed in the same manner as was done by Judge (1994).[3] The inferred electron densities are simply those values of the densities that match the observed ratios from a

[3] In all calculations, we used intersystem line oscillator strengths from Fang et al. (1993) and collisional rate coefficients from Blum & Pradhan (1992). Both of these have quoted uncertainties of $\pm 10\%$.

TABLE 3

STELLAR RADIAL VELOCITIES AND DOPPLER SHIFTS

Target	$V_{\rm Phot}$ (km s^{-1})	$V_{\rm C\,II} - V_{\rm Phot}$ (km s^{-1})
γ Dra	−27.6	+2.6 ± 3
α Tau[a]	+54.3	+3.9 ± 3
	+54.3	+3.9 ± 1.7
	+54.3	+5.2 ± 3
	+54.3	+3.9 ± 3
	+54.3	+9.0 ± 3
γ Cru.....	+21.4	+2.6 ± 3
μ Gem	+54.8 v	−2.6 ± 3
g Her	+3.4 v	−1.3 ± 3
λ Vel	+18.4	+2.6 ± 3
α Ori[a]	+21.0: v	+1.3:
	+21.0: v	0.0:
TX Psc	+18: v	−6.4:
RR Tel[b].....	−61.8 v	+3.9 ± 3

NOTES.—Uncertainties are typically 1 km s^{-1}, except for those targets with a "v" in the second column that indicates that the star is a photometric variable. A colon indicates an approximate value (the SIMBAD database contains very different velocities from different epochs and observers).

[a] Multiple rows for the same star correspond to the same rows in Table 2.

[b] This target was chosen as a control experiment; see text.

plot of ratio versus density.[4] Ratios R_1, R_2, and R_3 are sensitive to the electron density N_e of the emitting plasma. Ratios R_4 and R_5 should be constant, close to values of 7.28 and 1.04, respectively, if the atomic data were ideal and the line-formation calculations realistic. Data are shown for just two target stars. The remainder of the stars exhibit very similar behavior. In generating this figure, special care was taken to propagate errors correctly, since the derived ratios are very sensitive to errors due to photon counting statistics, inaccurate subtraction of fluxes of blended lines,[5] and other systematic sources of error (such as inaccurate laboratory wavelengths). The lowest panels show only those ratios between each line profile that have an estimated signal-to-noise ratio in excess of 20. The figure shows that the data are consistent with the idea that the electron densities are systematically higher on the red sides of the line profiles. This is seen in all target stars with the exceptions of the control target RR Tel and those noted below.

2.4. *Special Cases*

The supergiants α Ori and λ Vel present us with special cases. The blended line profiles are simply too broad to allow a reasonable subtraction of the blended lines, especially the strong line of Fe II (see Fig. 1). This blending problem is sufficiently serious that gradients in line ratios like those shown in Figures 3 and 4 should not be overinter-

[4] The poorly posed nature of the inverse problem (see, e.g., Judge, Hubeny, & Brown 1997) precludes assigning a given density to a given Doppler shift, so these densities cannot be taken literally.

[5] Some subjective judgement had to be exercised in estimating the noise across line profiles affected by blends since the physical effects of blended lines are likely to be different from the simple subtraction treatment used. Our approach was to scale up by an arbitrary factor of 5 the estimated errors introduced into a given line profile from the subtraction of the blended line before adding these to the errors computed from the line profiles without the blend. This basically flagged data points that are strongly influenced by blends.

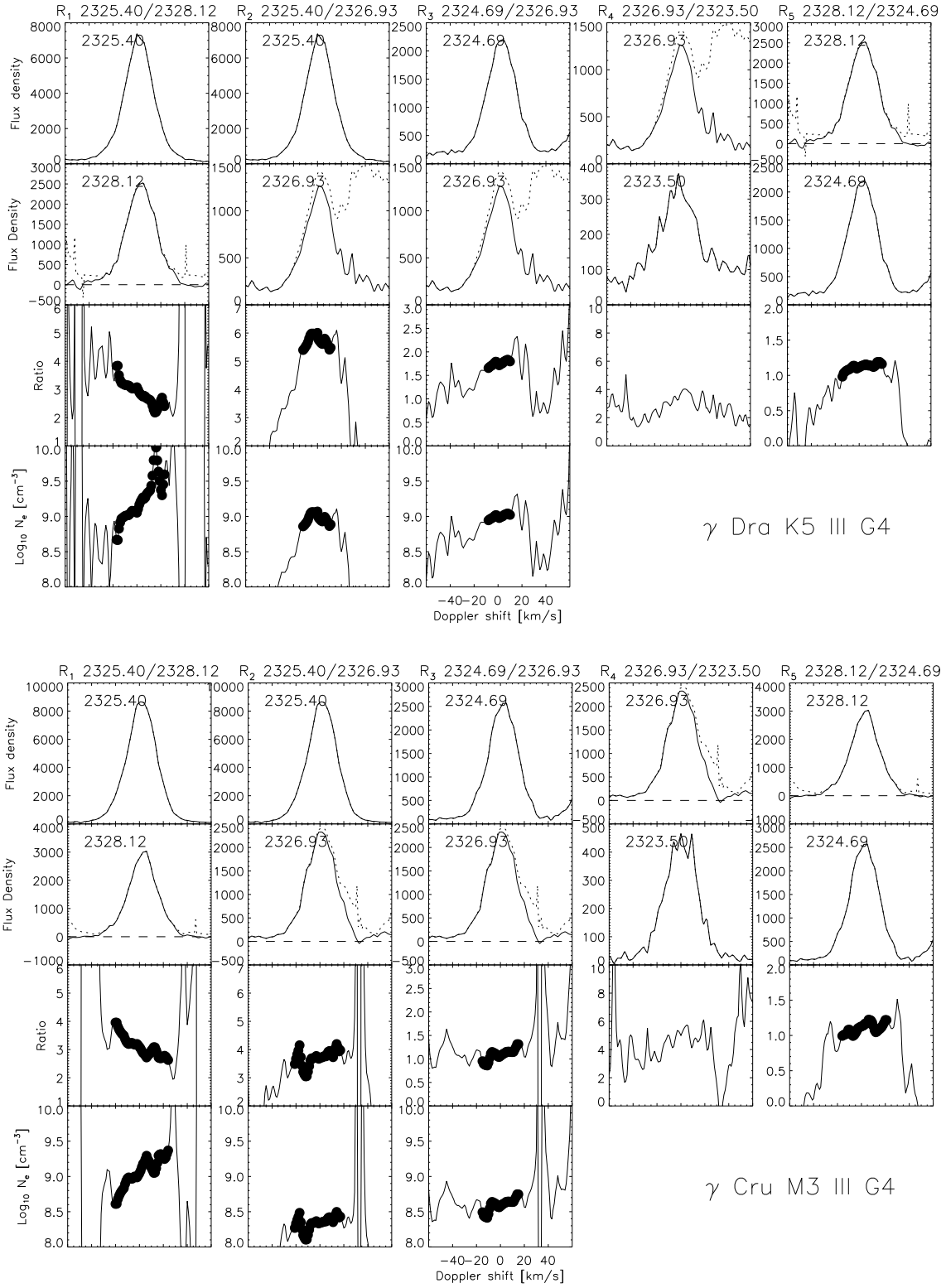

FIG. 3.—Line profiles, ratios of line profiles, and deduced electron densities plotted as functions of wavelength from line center, expressed in Doppler units of km s^{-1}. The unit of flux density is counts per diode on the detector. The solid lines in the line profiles (the upper two panels for each star) have blends removed; the dashed lines show the raw data including blends. All are shown in the rest frame of the stellar photosphere. Ratios R_1, R_2, and R_3 are sensitive to the electron density N_e, but ratios R_4 and R_5 are not. Data are shown for γ Dra and γ Cru. The heavy dotted symbol flags data that are believed to be reliable—other areas indicate the derived ratios but they are less reliable owing to poor signal-to-noise ratios and/or large influence of blended lines (see text).

preted. Further evidence that the ratios in supergiant stars should be treated with care is found below.

While the blends seriously influence the monochromatic flux densities, the wavelength-integrated flux densities are less affected. The three wavelength-integrated ratios observed in the spectra of α Ori imply electron densities that are far less consistent with each other than in the other stars, with R_2 indicating a $\log_{10}(N_e)$ as low as 7.5–8.0,

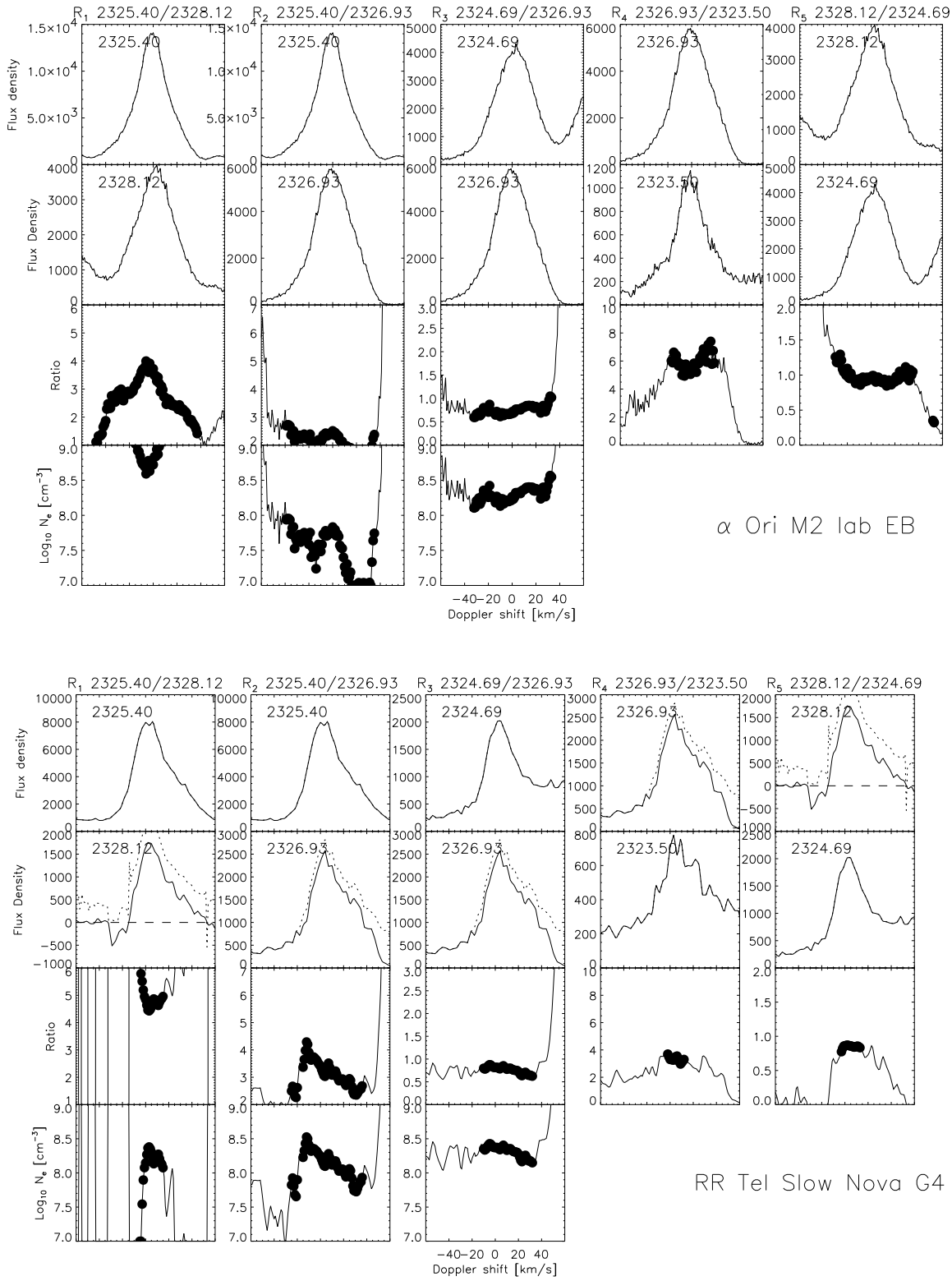

FIG. 4.—Similar to Fig. 3 for the supergiant α Ori and the slow nova RR Tel. For reasons discussed in the text, the lower panels for α Ori show data with no corrections for blended lines.

versus the 8.5–9.0 indicated by R_1 and the 8.0–8.5 implied by R_3 (see the lowest panels in the upper portion of Fig. 4). A possible explanation may be found in the Appendix, which discusses the effects of radiative transfer on the C II lines.

The targets μ Gem and TX Psc also present special problems since their spectra have insufficient signal-to-noise ratios to permit analysis of their line ratios. Nevertheless, their line widths are similar to those of the other stars, and the former does have enough counts to suggest a similar profile behavior to the other stars. As noted above, there is evidence of absorptions overlying the 2325.4 Å line of TX Psc. The strong absorption on the violet side of the emission line is at least partly caused by a line of Fe I (UV 13), which

absorbs C II photons and produces fluorescent emission and is seen only in carbon stars, in the Fe I (UV 45) line at 2807 Å (Carpenter et al. 1997). The absorption on the red side of the C II line remains unidentified. The presence of such absorptions invalidates the entire method of inferring electron densities from line ratios.

Finally, RR Tel is our "control" case, in the sense that the C II emission is emitted by a photoionized plasma and not one heated by the chromospheric heating mechanism(s). Figure 4 shows the line ratios for this case. While detailed interpretation of the data shown is difficult (the Large Science Aperture was used to acquire these data and so there is a convolution of source structure on the sky and spectral information), the figure illustrates one important point. The ratios R_1, R_2, and R_3 are all consistent with one another to within error estimates, which suggests that errors in laboratory wavelengths are not responsible for the systematic changes in the profiles of the other sources (see the Appendix of Judge et al. 1998 for a discussion of how these errors can propagate).

3. DISCUSSION

3.1. *Summary of Observations*

The observational results can be summarized as follows: the line profiles of intercombination lines of C II in a variety of normal giant and supergiant stars are broadened in excess of thermal broadening velocities and sound speeds; these profiles are, where accurate photospheric velocities are available, all significantly redshifted, but by substantially less than the observed line widths; the ratios of line profiles show differential changes with wavelength that, in comparison with ratios that are not sensitive to density and with ratios in the slow nova RR Tel, suggest that average electron densities are substantially higher in the plasmas emitting mostly on the red side of the line profiles; in the one target that has been observed repeatedly, these features all persist.

3.2. *Comparison with Models of Upward-propagating Shock Waves*

Not one of the above points is consistent with one-dimensional model calculations that are based upon acoustic heating, calculations that produce much narrower, blueshifted lines formed in gas with much higher electron densities in the upward-flowing parts of the chromosphere (Judge & Cuntz 1993). Thus, if we have correctly accounted for the formation of the C II spectrum in these stars, it appears either that something serious is missing from the acoustic models or that the whole picture is invalid.

Is it reasonable to argue that the picture is basically correct but that something is missing? There are several ways in which we can envisage the acoustic model being modified beyond what has been done in the simple calculations by Judge & Cuntz (1993), but none can reasonably be expected to solve the problem. First, the photospheric driver used by Judge & Cuntz (1993) is certainly too simple. However, it is hard to imagine any subsonic photospheric driver relying on hydrodynamics that can produce Mach numbers of several in the chromosphere, simultaneously leading to a net downflow of the most brightly emitting plasma. Essentially, all upward-propagating disturbances will lead to blueshifted emission.

Second, and more important, all earlier modeling work has been based upon one-dimensional calculations, whereas the generation and propagation of acoustic disturbances from the photosphere into the chromosphere is certainly three-dimensional. To address the question of the influence of three-dimensional gas dynamics, we must distinguish two cases: first, the case where there is zero magnetic field present; and second the case where magnetic fields, although weak, influence the gas dynamics at some height in the chromosphere.

In the first case, one can examine numerical simulations to analyze the likely nature of sources and propagation of acoustic-wave energy in the photosphere and chromosphere of the Sun. Recent simulations aimed at understanding the generation of sound waves indicate that significant sound wave generation is likely to occur in localized regions of high (>1) Mach number in surface layers (Bogdan, Cattaneo, & Malagoli 1993). Such sound wave generation must lead to substantial nonvertical (or nonradial) wave generation that may, when summed over stellar hemispheres, lead to substantial line broadening over and above what is calculated in one-dimensional models. However, such models could not be expected to lead to the observed asymmetries (the net redshifts and ratios seen in Fig. 3), at least in the statistical sample of observations examined here. Furthermore, the most complete one-dimensional calculations of acoustic heating in the Sun's "nonmagnetic" chromosphere indicate that, on average, the gas temperature decreases with height (Carlsson & Stein 1995). Thus, at least, linear waves would tend to be refracted toward the vertical by the decrease of sound speed with height in the photosphere/ chromosphere, making the one-dimensional approximation more appropriate. In this case, we would conclude that multidimensional effects cannot account for basic observed features of the observed line profiles.

In the second case, the situation is more complex. In unipolar magnetic field regions, the prevailing average magnetic field must be vertical or nearly so because of buoyancy forces. The propagation of three-dimensional acoustic fluctuations in the magnetic field thus tends to be fractionated by the magnetic field into fast- and slow-MHD modes. In a low-β plasma, the slow modes are field-aligned acoustic waves and are therefore effectively one-dimensional, as modeled by earlier authors. The fast modes travel almost isotropically but are preferentially refracted back toward the photosphere because of the exponential density stratification with height. Thus, the only surviving waves that are expected to propagate into the chromosphere are slow modes that are essentially one-dimensional field-aligned waves. In this case, we would conclude that our comparisons of observations with purely acoustic one-dimensional calculations are reasonable.

The final way in which we can envisage modifications to the model that can invalidate our analysis is that the formation mechanisms of these C II lines may be anomalous, and the acoustic mechanism survives to reproduce properties of the observed profiles. We suggest that this is unlikely because the lines are very broad, factors of several broader than the computations by Judge & Cuntz (1993). Nonequilibrium ionization will certainly alter the properties of the C II emission lines, but it is hard to imagine that such a radical discrepancy between the observed and computed line widths can arise unless such velocities are present in the atmospheric dynamics. In the Appendix, we argue that one potential culprit, the effects of radiative transfer on the line profiles, can (and does, at least for α Ori) influence the line

ratios, but it cannot account for the observed widths of the lines.

3.3. *Speculations Concerning the Origin of the* C II] *Line Profiles*

In a recent detailed study of the same transitions in O IV, Judge et al. (1998) found similar qualitative behavior in these lines formed in the quiet Sun's transition region. They argued that the solar data suggest that waves, if responsible for the line profile properties seen in O IV, must contain an important if not dominant compressive component that propagates *downward* from the corona. If confirmed by, for example, time-series observations, this requires the presence of a magnetic field to channel flows if not to drive them, and, in any case, the morphology of intensity maps in such lines indicates the dominance of magnetic fields. This suggests that the phenomena responsible for the solar O IV and stellar C II emission line profiles are related and that the basal fluxes may be controlled by magnetic processes. We note that, in the case of cool giant stars, the absence of much coronal material implies that the magnetic fields, if closed, will be filled mostly with cool material below the 10^5 K peak in the radiative-loss curve. Thus, such loops would be expected to be analogous to the "cool loop" solutions proposed by Antiochos & Noci (1986). Calculations are needed to determine if magnetic reconnection of the type envisaged by Parker (1988) and simply modeled by Wikstøl et al. (1997) can produce the type of dynamics necessary to reproduce the kinds of profiles seen here, or whether an entirely different class of model applies.

There is circumstantial evidence from other sources that suggests that magnetic fields may be important in controlling some aspects of the evolution of the stellar envelopes. For instance, some OH-IR stars such as VX Sgr have in their circumstellar shells detectable magnetic fields of a magnitude suggesting that magnetic fields are important in even later phases of stellar evolution than those studied here (see, e.g., Chapman & Cohen 1986). Perhaps more directly, an analysis of time-series chromospheric line data (of Mg II emission lines observed with *IUE*) of the "basal-flux" star β Hydri by Dravins et al. (1993) indicates that a substantial, presumably magnetic, activity cycle is present over a 12 yr period.

3.4. *Evidence that the Proposed Solar Basal Component Is Not Acoustic*

While not the subject of the present paper, our findings prompted us to examine solar data obtained by Carlsson, Judge, & Wilhelm (1997) with the SUMER instrument on the *SOHO* spacecraft. These data cast further doubt on the validity of the acoustically heated model of basal fluxes.

Schrijver (1992; see especially his Tables 1 and 4) analyzed the statistical properties of *Skylab* data obtained with the SO55 spectrograph. He derived a "well-determined" basal intensity for the entire C II λ1335 multiplet of 680 ergs cm^{-2} s^{-1} sr^{-1}, with an average quiet-Sun intensity of 1.5×10^3 ergs cm^{-2} s^{-1} sr^{-1}. Thus, the solar basal component for the C II λ1335 multiplet is $\sim$45% of its mean intensity.

Carlsson et al. (1997) studied SUMER time-series data of the 1334 Å component of the C II multiplet that cover an area of $120'' \times 10''$ of the quiet Sun. From an accompanying spectroheliogram, Carlsson et al. (1997) argued that this small region is typical of the quiet Sun, so it can reasonably be compared with the C II data analyzed by Schrijver (1992). The average (wavelength-integrated) intensity of the 1334 Å C II component along the slit gave rise to 72 counts s^{-1}, or 450 ergs cm^{-2} s^{-1} sr^{-1} using calibration data from Wilhelm et al. (1995). This implies an intensity of the whole multiplet of $\sim 1.03 \times 10^3$ ergs cm^{-2} s^{-1} sr^{-1}, using the observed $\lambda\lambda$1335/1334 ratio from Sandlin et al. (1986). This is comparable to the average value found by Schrijver (1992), confirming that the SUMER data are not atypical of the quiet Sun.

Consider the possibility that the acoustic component of chromospheric heating seen in the SUMER data consists entirely of the "Ca II grain" signature present in the UV continua and lines. Carlsson et al. (1997) showed that UV continuum variations related to the Ca II grain phenomenon can be seen over typically 50% of the area between chromospheric network. In their data, the time-averaged intensity of C II λ1334 in the area on the Sun showing Ca II grain behavior in the 1334 Å line yielded $\sim$20 counts s^{-1}, corresponding to $\sim$30% of the average intensity along the slit. However, the grains seen in C II occupy $\leq$20% of the whole area mapped by the SUMER slit (i.e., substantially less than the area showing grains in the UV continuum). Thus, these grains could contribute at most 6% to the C II intensity averaged along the slit in these SUMER observations. This must also be considered an upper limit estimate of the acoustic component to the intensity in these regions since Carlsson et al. (1997) found that theoretical calculations are able to account for only a fraction of the observed UV intensity. There is a pervasive "diffuse" component always present in the emission of lines and continua that is not even qualitatively accounted for in the model calculations. This fraction, estimated from the average to peak intensities and the duration of the grains as a function of time, is between one-half and one-third for continuum data and is probably less for C II. Thus, while more work is needed on larger data sets, these initial results suggest that less than 2%–3% of the average intensity in C II along the SUMER slit actually corresponds to that identifiable with the acoustic heating mechanism. This is an order of magnitude smaller than the fractional basal component identified by Schrijver (1992).

We conclude either that there is more acoustic heating than can be identified directly through recognition of grain-like phenomena in SUMER data, or that the statistical methods used by Schrijver (1992) have identified a basal component (probably including the diffuse component seen in SUMER data) that is not predominantly acoustic in nature.

3.5. *Reexamination of Earlier Evidence that Basal Fluxes Arise from Acoustic Mechanisms*

Let us assume that our basic conclusion is valid, that the basal components for chromospheric heating do not have an acoustic origin. Then it is important to reexamine the earlier evidence in support of an acoustic origin for chromospheric heating.

In the Sun, the basal levels of chromospheric emission cannot currently be compared with observations and models based upon acoustic heating. The primary lines that have been used, through radiation hydrodynamic simulations, to reveal the presence of upward-propagating acoustic shocks are the Ca II H and K lines (Carlsson & Stein 1994, 1997). In solar-like stars, the basal flux measured in

the Ca II H and K lines from Mount Wilson data is consistent with a radiative equilibrium atmosphere (see the coincidence of lines 1 and 5 in Fig. 1 of Rutten 1986). Thus the Mount Wilson data cannot be used to confirm or deny any relationship between basal fluxes and acoustically heated regions of the Sun's chromosphere identified through detailed observations and simulations—i.e., through the Ca II grains. Our analysis of solar C II lines in fact suggests that the measured basal component is an order of magnitude larger than that which can be accounted for by identifiable grainlike behavior.

In stars, the primary evidence that the basal component has an acoustic origin comes from comparisons of basal fluxes in Mg II $h + k$ lines and approximate calculations of acoustic fluxes generated by convection (Bohn 1984), coupled with detailed computations of chromospheric line fluxes (see, e.g., Buchholz & Ulmschneider 1994). Both are computed as functions of stellar gravity, effective temperature, and (in some cases) metallicity. Such models can reproduce the observed dependence of basal fluxes on these parameters remarkably well (Buchholz & Ulmschneider 1994) and have been cited as important evidence of acoustic shock waves as a chromospheric heating mechanism. Our major criticisms of this work are that comparisons of the spectra predicted by such models with observations sensitive to the shock dynamics reveal serious problems (Judge & Cuntz 1993; also see the present paper), and that the treatment of the generation of sound waves by convective envelopes is seriously compromised by application of a low Mach-number theory to high Mach-number regimes (see Bogdan et al. 1993).

4. CONCLUSIONS

We have argued that much of the evidence that is cited in support of an acoustic mechanism for heating of the basal components of stellar chromospheres is of an indirect, circumstantial nature. We therefore examined data of stars whose chromospheric activity levels are basal. We found that high-quality chromospheric line profiles have characteristics that are demonstrably inconsistent with the acoustic mechanism—the lines are far too broad, they have a net redshift in the rest frame of the star, and the line profiles are more characteristic of *downward* compressive wave propagation.

To reconcile our analysis with the current picture (as summarized by Schrijver 1995), we see several possibilities. First, our stellar targets may be pathologically different; after all, their status as basal is based upon flux-color diagrams (see, e.g., the surface flux of Mg II emission lines versus $B-V$ in Fig. 5 of Schrijver 1995 for example) and an extrapolation of the analysis of flux-flux diagrams (Fig. 4 of Schrijver 1995). If this were true, we would conclude that red giants simply appear to be basal but are actually heated by magnetic processes, and that the basal levels of the Sun (and solar-type dwarf stars) are still heated acoustically. Second, there may be some pathological problem with our choice of spectral lines—Judge (1994) discussed some of these aspects and concluded that there is nothing exceptional about C II lines in comparison with, for example, Mg II. Third, our analysis of the effects of radiative transfer in these particular lines may be grossly oversimplified (see the Appendix). Fourth, the gas dynamics may be much more complex than we anticipate, involving poorly understood processes such as convective overshoot in three dimensions. Any of the above possibilities would nullify our basic conclusion and therefore the acoustic mechanism for chromospheric heating would remain a viable mechanism for basal flux stars.

However, the final and most important possibility is that there is nothing unusual about our target stars and analysis and that, therefore, basal heating mechanisms across the H-R diagram are not consistent with the acoustic heating mechanism. This is in direct contradiction to earlier work. The resolution of this issue deserves serious attention in future work.

This research utilizes data from *HST*-GO programs 4685, 5358, 5359, 5694, 5863, 6068, and 6722, and is thus sponsored in part by NASA through STScI grants for these programs. We heartily thank R. Robinson for his work on the original reduction and calibration of these data. Tom Bogdan and an anonymous referee are gratefully acknowledged for suggestions that greatly improved the manuscript.

APPENDIX

EFFECTS OF RADIATIVE TRANSFER ON C II LINES

Potentially important effects of radiative transfer (RT) on the C II lines have been discussed by Judge (1994) in the context of α Tau. Judge argued that RT effects are probably negligible for the interpretation of the lines for that particular star. However, there are several reasons to reexamine this. First, our targets include supergiant and carbon star spectra—these stars have much lower surface gravities g than does α Tau (see, e.g., Judge & Stencel 1991), and chromospheric scaling laws (Ayres 1979) indicate that the column mass (and hence optical depth) m_* of the chromosphere scales like $g^{-1/2}$. Second, the line ratios in α Ori depart from theoretical calculations that assume that the emitting plasma is optically thin (compare the derived densities in α Ori and RR Tel shown in and lowest panels of Fig. 4). The three density-sensitive ratios do not agree with one another in the sense of yielding even approximately the same density (this was first recognized by Stencel et al. 1981 and was emphasized in radiative transfer work by Hartmann & Avrett 1984; it has remained something of a puzzle ever since). Third, ratio R_4 departs significantly from the optically thin limit in all target stars, which may be influenced by the effects of finite optical depths in the lines.

We consider the hypothesis that a significant optical depth is present in the C II intercombination line–forming regions of α Ori. The effects of multiple scattering of line photons are to force photons emitted close to line center to the line wings and to alter the relative fractions of photons escaping in lines sharing a common upper level. The simplest possible approximation that can qualitatively account for these effects is the "mean escape probability approximation" (see, e.g., Judge 1990, and references therein). While it can never reproduce the nonlocal nature of line transfer, the approximation can be used to

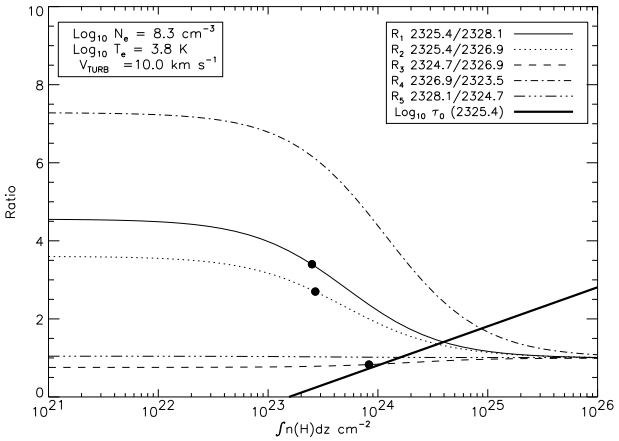

FIG. 5.—Line ratios between intercombination lines of C II as a function of column density of hydrogen (cm^{-2}) for fixed electron density ($N_e = 2 \times 10^8$ cm^{-3}), temperature ($\log_{10} T_e = 3.8$ K), and microturbulent velocity (10 km s^{-1}). Significant (>10%) departures from the optically thin limits occur for column densities in excess of 10^{23} cm^{-2}. The figure also shows the line center optical depth, which reaches values ≥ 1 at column densities $\geq 10^{24}$ cm^{-2} in the most opaque line (2325.4 Å). Filled circles show the observed line ratios in α Ori plotted with values on the abscissa chosen to make the observed and theoretical ratios equal.

indicate the qualitative effects in both line widths and ratios of integrated flux densities of emission lines (see, e.g., Osterbrock 1962) and is justified here only in the sense that more detailed transfer calculations require model atmospheres including realistic solutions for the energy and momentum equations. The availability of such models would negate the need for the present paper.

First consider the theoretical ratios of the frequency-integrated line fluxes. Figure 5 shows results of a mean escape probability calculation where the electron density, temperature, and "microturbulent" velocity are held fixed and the column density of the emitting plasma is varied. Zero incident radiation was included in the calculations, except that photoionization was implicitly assumed to produce C II as the dominant ionization stage. The figure shows that line ratios depart from their optically thin limit for hydrogen column densities in excess of 10^{23} cm^{-2} (a logarithmic solar abundance of carbon of 8.67, where the abundance of hydrogen is 12, was used, with all carbon assumed to be in the singly ionized form). This corresponds to the column density at which the strongest line, at 2325.4 Å, becomes optically thick ($\tau_\nu = 1$ at line center). The effects of increasing the hydrogen column density on the line ratios are to force all ratios closer to unity, lowering ratios R_1 and R_2 and slightly raising R_3. This is exactly what is needed to explain the "disagreements" between the three observed line ratios and a theoretical spectrum dominated by a plasma at a single density.

Averages of the observed ratios ($R_1 = 3.4$, $R_2 = 2.7$, and $R_3 = 0.83$) are shown as filled circles in Figure 5, in which the values on the abscissa are chosen to match the theoretical and observed values of the ratios on the ordinate. These represent typical observed values since they are the average values of the integrated line flux ratios in *IUE* spectra (Carpenter 1984) and in the GHRS data discussed here. The figure simply shows that the three observed ratios can be brought into "agreement" with a plasma emitting with one characteristic density, temperature, and column density.

Figure 6 shows results of calculations similar to those of Figure 5 except that the electron density was varied while holding the hydrogen column density fixed at values of $10^{23.5}$ and 10^0 cm^{-2}. Again, observed ratios are shown as filled and open circles for the high– and low–column density calculations, respectively. These figures suggest that the "discrepant" line ratios

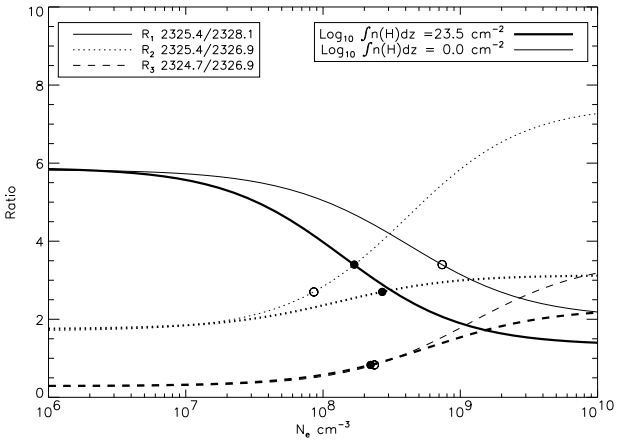

FIG. 6.—Similar to Fig. 5 except that the electron density was varied while holding the hydrogen column density fixed at a value of 1 (*thin lines*) and $10^{23.5}$ cm^{-2} (*thick lines*). The electron densities implied by the observed ratios R_1, R_2, and R_3 (see Table 1) of the flux densities fall into much better agreement with one another in the optically thick case than the optically thin case. Circles show the observed line ratios in α Ori plotted with values on the abscissa chosen to make the observed and theoretical ratios equal, for the high– (*filled circles*) and low–column density (*open circles*) cases.

can be reconciled most simply if the C II emission lines are formed in a region characterized by a single value of $N_e \sim 10^{8.3}$ cm^{-3} for the electron density if the mean hydrogen column density of the emitting plasma is $\int n(\mathrm{H})dz \sim 10^{23.5}$ cm^{-2}. The optical depth at the center of the line at 2325.4 Å is then ~ 2. Are such high column densities reasonable? These correspond to column masses of ~ 1 g cm^{-2}. In the model chromosphere of Hartmann & Avrett (1984), the temperature minimum is close to a column mass of 10 g cm^{-2}, but the electron temperature close to 1 g cm^{-2} is very low in this particular model, ~ 3500 K. Thus, little excitation of the C II lines is expected in this model. Nevertheless, in many regards, the model falls short of reproducing the observed spectra. Given the known complexity of the chromosphere of α Ori, we regard our hypothesis as reasonable.

Can these optical depths also broaden the lines sufficiently to invalidate our claim that the observed lines are just too broad to be consistent with models based upon outward-propagating shocks? The answer is no. To account for the observations, one must invoke more substantial optical depths in the lines themselves to force photons further away from the Doppler core. If transfer remains confined to the Doppler core (a good approximation for these lines), the lines if broadened above their optically thin value by a factor x would require line center optical depths τ_0 such that $(\ln \tau_0)^{1/2} \sim x$ (see, e.g., Osterbrock 1962). For $x \sim 2$, implied by the arguments given above, $\tau_0 \sim 55$. Such high optical depths are not consistent with the observed ratios of the lines (see Fig. 5) and would place the line formation in the photosphere of the model by Hartmann & Avrett (1984).

We conclude that optical depths are high enough in the chromospheres of α Ori to influence the line ratios and thereby render all conclusions based upon the assumption of optically thin line formation invalid for these lines. Thus, one cannot trust the dependence of line ratios on Doppler velocity for α Ori, and one must be wary of similar effects for the other stars with the lowest gravity among our targets (g Her, TX Psc, λ Vel). We also conclude that the optical depths are insufficient to broaden the lines significantly. Chromospheric scaling laws would suggest that our assumptions of negligible optical depth in the C II lines is valid for the giant stars in our sample, as found by Judge (1994).

One interesting problem with ratio R_4 remains. The measured ratios R_4 for all stars lie between 3.5 and 7, consistently lower than the computed values. There are three possibilities that might account for the discrepancy: (1) the optical depths are high enough [$\int n(\mathrm{H})dz \sim 10^{24-24.3}$ cm^{-2}] to produce ratios closer to 1:1 (see Fig. 5); (2) the atomic data are in error and the branching ratio is closer to 3.5–5 than to 7; and (3) the 2323.5 Å line is weak and its flux density is systematically influenced by inadequate treatment of continuum and or blended-line emission. We discount (1) since the measured ratio shows no systematic dependence on gravity; furthermore, it would require line formation in the photospheres of the giant target stars. The other possibilities do not affect the overall analysis and can be ignored.

REFERENCES

Antiochos, S. K., & Noci, G. 1986, ApJ, 301, 440
Ayres, T. R. 1979, ApJ, 228, 509
Ayres, T. R., Marstad, N., & Linsky, J. L. 1981, ApJ, 247, 545
Blum, R. D., & Pradhan, A. K. 1992, ApJS, 80, 425
Bogdan, T. J., Cattaneo, F., & Malagoli, A. 1993, ApJ, 407, 316
Bohn, H. U. 1984, A&A, 136, 338
Buchholz, B., & Ulmschneider, P. 1994, in ASP Conf. Proc. 64, Eighth Cambridge Workshop on Cool Stars, Stellar Systems, and the Sun, ed. J.-P. Caillault (San Francisco: ASP), 363
Carlsson, M., Judge, P. G., & Wilhelm, K. 1997, ApJ, 486, L63
Carlsson, M., & Stein, R. F. 1994, in Proc. Mini-Workshop on Chromospheric Dynamics, ed. M. Carlsson (Oslo: Inst. Theor. Astrophys.), 47
———. 1995, ApJ, 440, L29
———. 1997, ApJ, 481, 500
Carpenter, K. G. 1984, ApJ, 285, 181
Carpenter, K. G., Robinson, R. D., Johnson, H. R., Eriksson, K., Gustafsson, B., Pijpers, F. P., Querci, F., & Querci, M. 1997, ApJ, 486, 457
Chapman, J. M., & Cohen, R. J. 1986, MNRAS, 220, 513
Dravins, D., Linde, P., Fredga, K., & Gahm, G. F. 1993, ApJ, 403, 396
Fang, Z., Kwong, V., Wang, J., Parkinson, W., & Smith, P. 1993, Phys. Rev. A, 48, 1114
Hartmann, L., & Avrett, E. H. 1984, ApJ, 284, 238
Heap, S. R., et al. 1995, PASP, 107, 871
Holzer, T. E., & MacGregor, K. B. 1985, in Mass Loss from Red Giants, ed. M. Morris, B. Zuckerman (Dordrecht: Reidel), 229
Judge, P. G. 1986, MNRAS, 223, 239
———. 1990, ApJ, 348, 279
———. 1994, ApJ, 430, 351
Judge, P. G., & Cuntz, M. 1993, ApJ, 409, 776
Judge, P. G., Hansteen, V. H., Wikstøl, Ø., Wilhelm, K., Schühle, U., & Moran, T. 1998, ApJ, submitted
Judge, P. G., Hubeny, V., & Brown, J. C. 1997, ApJ, 475, 275
Judge, P. G., & Stencel, R. E. 1991, ApJ, 371, 357
Oranje, B. J. 1986, A&A, 154, 185
Osterbrock, D. E. 1962, ApJ, 135, 195
Parker, E. N. 1988, ApJ, 330, 474
Rutten, R. G. M. 1986, A&A, 159, 291
Rutten, R. G. M., & Pylyser, E. 1988, A&A, 191, 227
Rutten, R. G. M., Schrijver, C. J., Lemmens, A. F. P., & Zwaan, C. 1991, A&A, 252, 203
Sandlin, G. D., Bartoe, J.-D. F., Brueckner, G. E., Tousey, R., & VanHoosier, M. E. 1986, ApJS, 61, 801
Schrijver, C. J. 1987, A&A, 172, 111
———. 1992, A&A, 258, 507
———. 1995, A&A Rev., 6, 181
Smith, M. A., & Dominy, J. F. 1979, ApJ, 231, 477
Soderblom, D. R. 1993, BAAS, 183, 1714
Stencel, R. E., Linsky, J. L., Brown, A., Jordan, C., Carpenter, K. G., Wing, R. F., & Czyzak, S. 1981, MNRAS, 196, 47P
Ulmschneider, P. 1991, in Mechanisms of Chromospheric and Coronal Heating, ed. P. Ulmschneider, E. Priest, & B. Rosner (Berlin: Springer), 328
Wikstøl, Ø., Judge, P. G., Hansteen, V. H. 1997, ApJ, 483, 972
Wilhelm, K., et al. 1995, Proc. SPIE, 2517, 2
Wilson, R. E. 1963, General Catalogue of Stellar Radial Velocities, Mount Wilson Observatory Technical Report 601 (Washington, DC: Carnegie Instit. of Washington)